Biosensors and Bioelectronics 129 (2019) 269–276

Contents lists available at ScienceDirect

Biosensors and Bioelectronics

journal homepage: www.elsevier.com/locate/bios

Detection of bacterial metabolism in lag-phase using impedance spectroscopy of agar-integrated 3D microelectrodes

Derrick Butler[a,b], Nishit Goel[a,b], Lindsey Goodnight[a,b], Srinivas Tadigadapa[c], Aida Ebrahimi[a,b,*]

[a] School of Electrical Engineering and Computer Science, Pennsylvania State University, University Park, PA 16802, United States
[b] Materials Research Institute, Pennsylvania State University, University Park, PA 16802, United States
[c] Department of Electrical Engineering, Northeastern University, Boston, MA 02115, United States

ARTICLE INFO

Keywords:
Bacteria
Metabolism
Impedance sensing
Gold nanostructures
Gel medium

ABSTRACT

Traditional methods for detection of metabolically-active bacterial cells, while effective, require several days to complete. Development of sensitive electrical biosensors is highly desirable for rapid detection and counting of pathogens in food, water, or clinical samples. Herein, we develop a highly-sensitive non-Faradaic impedance sensor which detects metabolic activity of *E. coli* cells in a mere 1 μl of sample volume and without any sample filtration/purification. The three dimensional (3D) interdigitated electrodes (IDEs) along with self-assembled gold-nickel (Au-Ni) nanostructures significantly amplify the sensitivity by increasing the sensing area almost three-fold. The developed microsystem is integrated with an agar-based growth medium and monitors the metabolism of bacterial cells, enabling bacterial detection in approximately one hour after inoculation, i.e. in the lag-phase. Incorporation of a secondary agar layer as a biocompatible passivation layer protects the IDEs from potential Faradaic reactions and enhances sensitivity to modulation of the non-Faradaic impedance due to cellular metabolism. The resultant label-free sensor is capable of selective identification of metabolizing cells (vs. dead cells) across a wide linear range (10–1000 cells/μl). These results help pave the way for rapid antibacterial susceptibility testing at the point-of-need, which is currently a major challenge in healthcare.

1. Introduction

Metabolic activity is a very important characteristic when analyzing viability of bacterial cells, such as *Escherichia coli* (*E. coli*). *E. coli* is the most common cause of urinary tract infections (UTI) in humans, and cost > $2 billion in the United States during 2010 (Foxman, 2014). The total number of bacterial cells, irrespective of their type, is usually an indication of the quality of water, food, and clinical samples. Hence, an analytical method that can detect live (more precisely, metabolizing) cells at the point-of-need is highly desirable. The gold standard methods (e.g. colony counting method) for indiscriminately quantifying live cells are very sensitive and cost-effective. However, they suffer from long incubation times (at least 24–72 h) which is required to reach a certain threshold before the signal (usually optically/visually) can be detected.

Among different methods for quantifying live cells, impedance microbiology (IMB) is of particular interest due to cost-efficiency and simple readout as these methods are readily compatible with integrated circuit (IC) technology. IMB monitors the electrical characteristics of bacterial culture medium changed as a result of the release of ionic metabolites from live cells (Gómez-sjöberg et al., 2005). If the impedance changes beyond a specific threshold, a positive signal is detected. Impedimetric biosensors are used for various applications including detection of DNA hybridization (Ebrahimi and Alam, 2015; Kurkina et al., 2011; Xu et al., 2004), cell culturing (Ebrahimi and Alam, 2017; Yang and Bashir, 2008), monitoring of cell migration (Bajwa et al., 2013), on-chip probing of activation of bacterial ion channels (Ebrahimi et al., 2018; Ebrahimi and Alam, 2016), and pathogen detection (Mannoor et al., 2010; Sidhu et al., 2016).

Although they offer simple instrumentation and real-time analysis, the detection time of the conventional IMB methods for enumerating metabolizing cells can be very long. There is a logarithmic dependence between the initial cell concentration and detection time, i.e. the lower the initial cell concentration, the longer the detection time. For example, detection of cells such as *E. coli* (one of the fastest growing bacterial cells) with an initial concentration of 10 cells/μl takes at least 4 h to complete using conventional IMB methods (Gómez et al., 2002). Moreover, most of the existing IMB methods require a change of the testing medium (to minimize the background noise), and hence may not comply with the standard methods in the industry (e.g. the colony counting method (Balestra and Misaghi, 1997)). As such, it is highly

* Corresponding author at: School of Electrical Engineering and Computer Science, Pennsylvania State University, University Park, PA 16802, United States.
E-mail address: sue66@psu.edu (A. Ebrahimi).

https://doi.org/10.1016/j.bios.2018.09.057
Received 30 June 2018; Received in revised form 10 September 2018; Accepted 16 September 2018
Available online 17 September 2018
0956-5663/

desirable to develop a platform that combines the advantages of impedance spectroscopy with colony counting method (Bajwa et al., 2013).

In this work, we present a highly-sensitive impedimetric biochip which detects metabolic activity of 10–10^3 cells/μl (equivalent to 10^4-10^6 cells/ml) of *E. coli* cells in 1 μl of sample volume, in one hour. The system comprises of two chips: a sensing chip and a seeding chip. The sensing chip integrates two 3D IDEs with self-assembled gold-nickel (Au-Ni) nanostructures to significantly enhance the sensitivity. The seeding chip consists of a bilayer of agar gels: a thin passivation layer (DI-agar) and a nutrient agar layer (BHI-agar) as the solid medium necessary for in situ bacterial culture. The compact design of the integrated chip enables localized diffusion of the ions that are released from cells as they metabolize. As a result, the detection time is significantly reduced compared to the existing IMB reports, from several hours to just one hour. Considering that the experimental setup and the sensing platform can be manufactured inexpensively, this work can open up new avenues for developing electronic platforms for rapid, high-throughput analysis of bacterial susceptibility to antibacterial treatment by integrating an array of antibiotic-containing agar pads.

2. Materials and methods

2.1. Fabrication of the sensing chip

Fabrication of the sensors starts with cleaning of glass slides in piranha solution (4:1 – H_2SO_4:H_2O_2) for 30 min to remove organic residues. After cleaning, a seed layer of Cr/Au – 10 nm/100 nm is deposited on the glass slides using electron-beam (e-beam) evaporation method. In order to define the interdigitated patterns, we use standard photolithography using photoresist SPR 220. Next, we electrodeposit Ni in High Speed Nickel Sulfamate Plating Solution (Technic Co.) with current density of ~ 6 mA/cm^2 for 125 min to get a ~ 10 μm thick layer. The photoresist layer is then removed after completion of electroplating, followed by chemical wet etching of the seed layer of Cr/Au to electrically separate the two IDEs. To enhance the surface roughness (and hence, the effective sensor area), the patterned 3D Ni electrodes are immersed in Bright Electroless Gold Plating Solution (Technic Co.) at 65 °C, as recommended by the manufacturer. We have studied the effect of the deposition time on the surface morphology and the surface wettability using Atomic Force Microscopy (AFM) and contact angle measurements, respectively.

2.2. Bacterial growth conditions and heat treatment

For this study, we used *E. coli* K12 which is one of the most-characterized *E. coli* models with biosafety level 1 properties (EPA, 1997), and there have been various reports on studying its antibiotic susceptibility (Nazemi et al., 2017; Creamer et al., 2017). From a frozen stock of *E. coli* K12, a loop-full is resuspended in the Brain Heart Infusion (BHI) medium, followed by overnight aerobic incubation (in the presence of oxygen) at 37 °C. Following serial dilution and plating on nutrient agar and overnight incubation, a single colony is isolated and inoculated in 5 ml of BHI and grown overnight. 100 μl of this culture is then inoculated into 10 ml of BHI and grown overnight at 37 °C with aeration (this is the initial culture). To prepare the working culture, depending on the desired concentration (ρ), we mix the cell suspension from the initial culture into fresh BHI in a microcentrifuge tube. To prepare dead cells, a microcentrifuge tube containing live cells is heated for 30 min in a water bath preset to 80 °C. 1 μl of the working culture (live or dead) with cell concentration of ρ is dropped onto the complete chip, followed by incubation at 37 °C with aeration. After certain incubation times, the impedance is measured.

2.3. Preparation of the seeding chip

The DI-agar and BHI-agar pads are prepared by mixing agar (from BDH Co.) with deionized (DI) water and BHI broth, respectively. The weight percentage (wt%) of agar in DI-agar and BHI-agar is 0.5% and 1.8%, respectively. After preparing the suspensions, the mixtures are autoclaved at 121 °C for 15 min. BHI-agar suspension is poured into a sterile petri dish with a thickness of ~ 1 mm. After solidification at room temperature, the gels are kept at 4 °C until the experiments. In order to prepare the sensing chip, the DI-agar is heated in a water bath (at 75 °C) until it is completely molten. 20 μl of the molten DI-agar is then dropped over the microelectrodes and allowed to solidify before placing the seeding chip (i.e. BHI-agar pads). BHI-agar pads with area of 2 × 2 mm^2 are cut using sterile cover slips.

2.4. Non-Faradaic impedance characterization

After preparation of the bacterial samples, the impedance measurements are carried out using an HP Agilent 4192A LF Impedance Analyzer with an auto-balance bridge and 1 m cable length. An AC signal of 50 mV is applied between the two IDEs and the frequency is swept from 300 Hz to 2 MHz, to understand how the impedance ($Z = Z_{Re} - jZ_{Im}$, where Z_{Re} and Z_{Im} are the real and imaginary part of the complex impedance, respectively) of the system (including electrodes, agar gels, and cells) changes in various frequency regimes. It should be noted that compared to Faradaic impedance sensing, non-Faradaic impedance measurement eliminates the need for applying a DC potential and hence, significantly reduces the power consumption. In addition, non-Faradaic measurements have the added benefit of not requiring redox probes or a reference electrode (which are usually challenging for miniaturization).

2.5. Electrochemical characterization of the electrode-agar interface

Cyclic voltammetry (CV) and electrochemical impedance spectroscopy (EIS) of bare IDEs (Ni and Au-Ni) and DI-agar (with wt% of 0.5% and 1%) biochips are performed in potassium ferricyanide (5 mM in PBS, pH 7.2; from Sigma Aldrich Co.) as the redox probe. We utilize a PalmSens4 potentiostat (PalmSens Co.) in a three-electrode configuration (with Pt counter electrode and a Ag/AgCl reference electrode). The data is collected using the proprietary PSTrace5 software. The CV and EIS measure the Faradaic reactions in order to probe the interface properties of the electrode-agar system. The EIS is performed by applying an AC signal of 10 mV and a DC bias of 0.25 V. The frequency is swept across a range from 10 mHz to 1 MHz. For the CV measurements, the voltage is swept at different scan rates from 50 mV/s to 200 mV/s in the potential range of −0.2 to 0.7 V. For both CV and EIS measurements, the contact pads of the sensor are covered with Kapton®, leaving only the IDE regions exposed to the solution.

2.6. Surface and contact angle characterization

In order to evaluate the effect of Au deposition time on the electrode surface roughness, four samples with different deposition times are prepared: Sample 1 with bare electrodeposited Ni and without any electroless Au deposition, Sample 2 with 5 min of electroless Au deposition, Sample 3 with 30 min of electroless Au deposition, and Sample 4 with 60 min of electroless Au deposition on top of Ni electrodes. By increasing the deposition time for electroless gold on the device, the amount of gold deposited increases which allows the size of the nanostructures of gold on the nickel electrodes to increase. We utilize a Bruker Icon 1 Atomic Force Microscopy (AFM) tool to map the surface profile and obtain the average roughness R_a for each of the four samples over an area of 5 × 5 μm^2. Contact angle measurements are carried out by carefully placing a ~ 5 μl droplet of DI water on samples and imaging the droplet profile at near 0° incidence angle using an optical

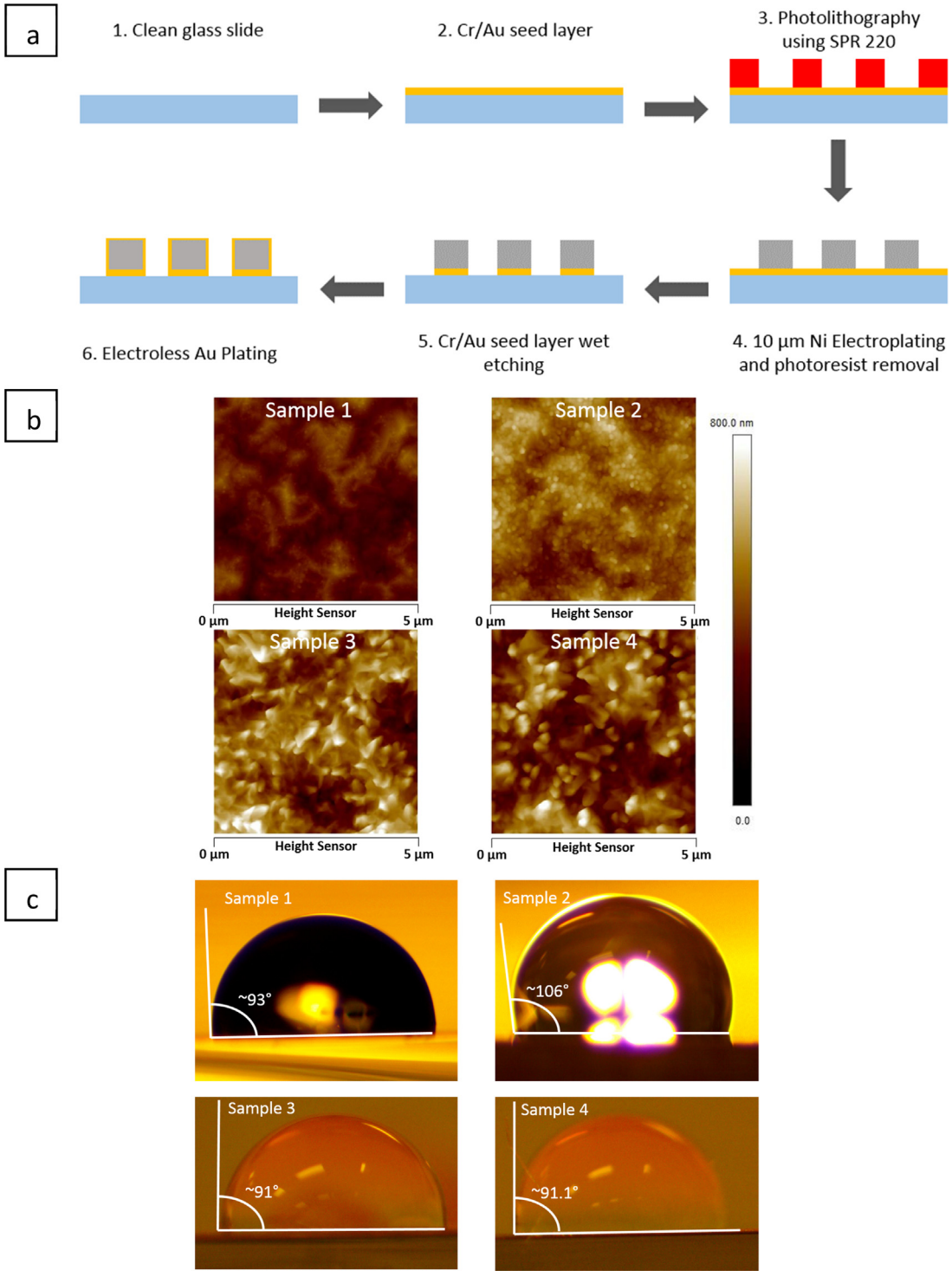

Fig. 1. (a) Schematic of device fabrication: (1) glass slides are cleaned in piranha solution, (2) Cr/Au seed layer is deposited by e-beam evaporation, (3) photolithography is used to define IDEs, (4) 3D Ni electrodes are electrodeposited followed by photoresist removal, (5) wet chemical etching is used to remove the seed layer, and (6) Au is deposited using electroless deposition method. (b) Atomic force microscopy images of four samples with Au deposition time of: 0 min, 5 min, 30 min, and 60 min, i.e. Samples 1–4, respectively. (c) Contact angle measurements on Samples 1–4.

camera (Amscope) mounted on a microscope (Leica SE6 Stereo Zoom).

3. Results and discussion

3.1. Understanding the parameters affecting the sensitivity

Fig. 1a illustrates the microfabrication process for the IDEs (i.e. the sensing chip). Briefly, a seed layer of Cr/Au is deposited on a glass slide by e-beam evaporation, followed by patterning of the IDEs using photolithography. Afterwards, the Ni layer (with thickness of h~10 µm) is electrodeposited. After removing the photoresist and the seed layer, we perform electroless deposition of gold. The final dimensions of the digits are h~10 µm, width w~15 µm, length L~2 mm, and inter-digit spacing of d~35 µm. Fig. 1b and c show the AFM images and contact angle images of the sensor surface before and after deposition of gold nanostructures for durations of 0 min, 5 min, 30 min, and 60 min,

designated as Samples 1 through 4, respectively. The surface morphology and wettability depend on the deposition time, as seen in Fig. 1b and c. The surface roughness increases from ~ 58 nm to ~ 109 nm with Au deposition time varying from 0 min to 60 min. The contact angle increases from 93° for bare Ni surface (Sample 1) to 106° after 5 min of Au deposition (Sample 2) which can be attributed to the formation of gold nanoclusters (see AFM images in Fig. 1b). However, increasing the deposition time from 5 min to 60 min leads to a reduction in the contact angle from 106° to 91°, even though the surface roughness has increased. This could be due to the fact that as the deposition time increases, the deposited gold forms microstructures, rather than nanostructures (Fig. 1b). This, in turn, leads to a reduction of the hydrophobicity of the surface, i.e. reduction of the contact angle. Hence, for the sensor fabrication, we deposit Au for 5 min to achieve higher hydrophobicity, which is important for controllable deposition of the DI-agar solution over the IDEs and achieving repeatable geometries from sample to sample (Ebrahimi et al., 2013).

The use of IDEs has become a commonplace for impedimetric biochemical sensors (Varshney and Li, 2009; Thomas et al., 2004; Ebrahimi et al., 2018). An IDE is comprised of a number of narrow, parallel electrodes with alternating electrodes connected. Due to the close spacing between the two IDEs (i.e. anode and cathode), they can cycle analytes back and forth between the electrode digits easily (Varshney and Li, 2009; Thomas et al., 2004). They also possess a relatively large surface area, making them very sensitive to minute amounts of target species. Moreover, micrometer-scale IDEs (as used in this work) enable slower depletion of the reactants compared to macroscale electrodes. This is due to the small spherical diffusion layer of microelectrodes, which contrasts to the semi-infinite diffusion layer of macroelectrodes (Min and Baeumner, 2004).

Here, Ni is chosen as the base electrode material due to its low cost and feasible electrodeposition process. Also, Nickel is widely used in coating industry due to its superior protection against corrosion (i.e. Faradaic reactions) (Aperador Chaparro and Lopez, 2007). However, Nickel has limited biocompatibility, making some potential applications, especially implantable devices, challenging (Bencko, 1983). Nickel can also oxidize easily in ambient environments (Cempel and Nikel, 2006). To address these challenges, we passivate the Ni IDEs with self-assembled Au nanostructures using electroless deposition. Au is a precious metal with an excellent biocompatibility (Shukla et al., 2005) and highly resistant against chemical or oxidative reactions, hence a suitable interface layer in electrochemical/electronic biosensors.

Compared to conventional IDEs with thin film electrodes, the 3D nature of our design enhances the total surface area by ~ 3×, which is further amplified by self-assembled Au nanostructures (an additional 51%). After the sensing chip is fabricated, we follow the experimental steps summarized in Fig. 2a-f. Briefly, in order to passivate the IDEs (i.e. the sensing chip) from potentially degrading Faradaic reactions, a thin layer of molten DI-agar is deposited (see Section 2 for details). The device is left at room temperature (RT) for the DI-agar gel to solidify. Then, the agar growth medium (a gel pad of 1.8% BHI-agar medium) is aligned and placed on IDEs, followed by deposition of 1 µl of sample suspension (i.e. live cells in BHI, dead cells in BHI, or cell-free BHI solution as control). The chip is then placed in the incubator and after certain incubation times, the non-Faradaic impedance is measured and compared with the control sample (the results discussed later). Before discussing the sensing performance for detection of bacterial metabolism, we will explain (i) how self-assembled Au nanostructures enhance sensitivity and (ii) why a DI-agar layer is incorporated in the biochip.

(i) In order to explain the role of Au nanostructures in improving the sensitivity, we performed CV analysis of the IDE electrodes before and after electroless deposition of Au. As depicted in Fig. 3a, the peak current, I_p (see arrows in Fig. 3a), increases significantly for Au-Ni IDEs compared to bare Ni IDEs. The increase in I_p indicates a larger available surface area according to the Randles-Sevcik equation (at RT) (Brownson and Banks, 2014.):

$$I_p = (2.68 \times 10^5) A n^{3/2} \vartheta^{1/2} D^{1/2} C, \quad (1)$$

where A is the electrode surface area, n is the number of electrons participating in the redox, D is the diffusion coefficient, ϑ is the scan rate, and C is the concentration of the analyte (here, the ferricyanide redox probe). Assuming the only variable that changes between the Ni IDE and the Au-Ni IDE is the surface area, A, we estimate the surface area increases by 51%. The improvement of peak current is consistent with increasing the surface roughness obtained using AFM (see Fig. 1b). The Au-Ni IDE also demonstrates a better anodic/cathodic peak current ratio when compared to the bare Ni IDE, indicative of better electrochemical reversibility (see SI (Supplementary information), Fig. S1). The peak oxidation currents scale linearly with the square root of the scan rate for all configurations (bare Au-Ni, and Au-Ni with DI-agar gel). This indicates a diffusion-limited process (see SI, Fig. S2).

(ii) To confirm the passivation properties of the DI-agar layer, we use EIS with a Fe^{3+}/Fe^{2+} redox probe (Fig. 3b). For non-Faradaic impedance measurements, it is desirable to reduce, and ideally eliminate, any Faradaic currents from contributing to the impedance (Dak et al., 2014). To realize this, a DI-agar gel is deposited onto the electrodes. Fig. 3b shows that the DI-agar gel limits charge transfer at the electrodes. For our system, we use Randles circuit model to analyze the charge transfer of Au-Ni IDE with and without the DI-agar layer. We extract the charge-transfer resistance (R_{ct}) by fitting a semicircle to the EIS data in the Nyquist plots. The diameter of this semicircle is the charge-transfer resistance (Zhang et al., 2005; Bard and Faulkner, 2001). R_{ct} values are shown for all four electrode configurations. When compared to the bare Au-Ni IDE, a 67% and 135% increase in R_{ct} are observed in samples with 0.5% and 1% DI-agar passivation layers, respectively. These results demonstrate that the addition of DI-agar causes a drastic reduction in the Faradaic component of the current (consistent with the CV data showing the near elimination of the anodic and cathodic peaks; see SI, Fig. S3). It should be mentioned that although the 1% DI-agar solution exhibits a greater charge transfer resistance, it can become more difficult to deposit the molten gel solution quickly without it solidifying in the pipette tip. It can also make diffusion of ions from the bacteria more difficult, therefore prolonging the detection time. As a result, 0.5% DI-agar gel is used for the rest of the study, unless otherwise stated.

3.2. Diffusing metabolites modify the impedance

Fig. 4a shows the optical image of an array of four biochips. The insets depict the IDEs before and after integration (bonding) with the seeding BHI-agar pad. Fig. 4b demonstrates the circuit model for the integrated system, including the IDEs, the passivation layer (DI-agar), the bacterial culture layer (BHI-agar), and bacterial cells. The interface between the IDEs and the medium is depicted by Z_{int} which contains the charge transfer resistance, R_{ct}, the double layer capacitance, C_{dl}, and the Warburg impedance, Z_W, representing mass transport. Z_W is dominant at low frequencies and hence can be neglected in the frequency range studied in this work. The medium, comprised of the stack of the BHI-agar and the DI-agar layers, can be modeled as parallel combination of dielectric capacitance, C_d, and the medium resistance, R_{series}. At relatively low frequencies (below 100 kHz), cells can be modeled as a resistance, R_{cell}, which increases with cell density, ρ.

Live bacteria have an intact cell membrane with protein channels that make the membrane semipermeable to diffusion of important solutes, such as ions (Levina et al., 1999). On the other hand, dead cells have a totally permeable cell membrane and can no longer control the uptake or release of ions and other solutes. This causes the content of the cell to leak through the cell wall and into the surrounding

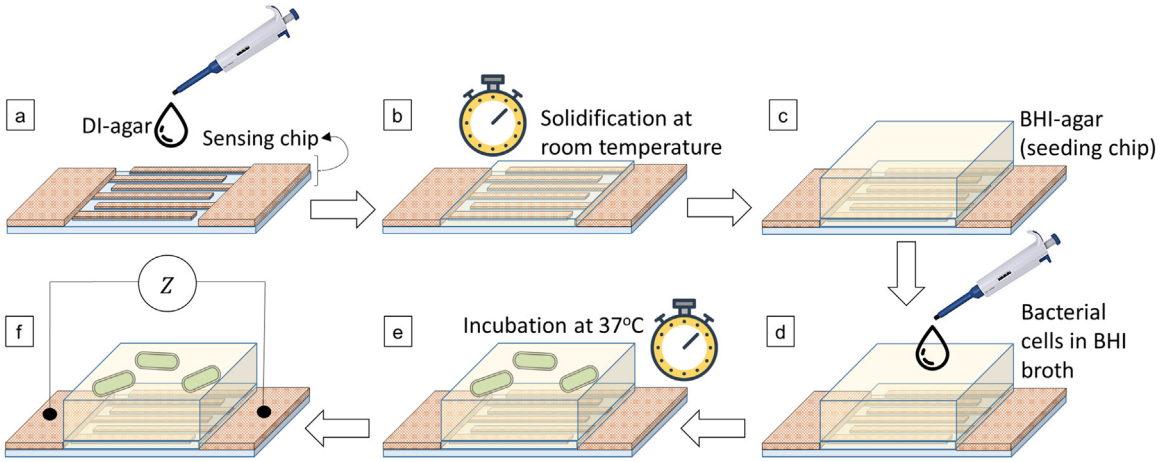

Fig. 2. Schematic of the experimental procedure: (a) drop-cast of 20 µl of molten DI-agar (the passivation layer) over the sensing chip, followed by (b) solidification of the passivation gel layer at room temperature. (c) A gel pad of BHI-agar is aligned and placed over the IDEs, (d) followed by pipetting of 1 µl of the sample solution with different cell concentration and/or viability. (e) The biochip is placed in a cell culture incubator and after specific incubation times (f) the non-Faradaic impedance is measured.

environment, resulting in a significant increase in the overall conductance (or decrease in the impedance) compared to live cells (Ebrahimi and Alam, 2016); see Fig. 5a and b comparing the impedance magnitude, $|Z|$, and phase, θ_Z, as a function of frequency for live and dead cells after 45 min incubation. Compared to both live and dead cells, the control sample (i.e. BHI broth) has the largest impedance, which is consistent with the above discussion. The difference in ion-concentration released by live vs. dead cells allows for the measurement of cell concentration based on variations in the impedance of the surrounding medium. At lower frequencies (10^2–10^3 Hz), $|Z|$ of all three samples is similar. This frequency regime is dominated primarily by capacitive terms (mainly C_{dl}). As the frequency increases, resistive components (R_{series} and R_{cell}) start to dominate. In this frequency range, we can distinguish $|Z|$ of the three samples. As expected, the diffusion of cytoplasmic species out of the heat-treated cells causes a large decrease of $|Z|$, compared to the BHI control sample. A smaller decrease in impedance can be seen in live samples, when compared to the BHI control, which is due to semipermeable nature of the cell membrane.

In order to determine the detection time of the biochip, time-dependent impedance measurements are performed with three different concentrations (10, 100, 1000 cells/µl) using live and dead cells (Fig. 6a). In order to quantify the relative change in the measured signal, we define a normalized differential impedance as,

$$\frac{\beta}{\beta_0} = \frac{1-\frac{|Z(t)|}{|Z_{BHI}(t)|}}{1-\frac{|Z(t_0)|}{|Z_{BHI}(t_0)|}}, \quad (2)$$

where $Z(t)$ and $Z_{BHI}(t)$ are the impedance for a given sample and BHI at time t, respectively. t_0 is the initial measurement time (in this work, t_0=15 min. A working frequency of 38 kHz is chosen to ensure that the resistive components are dominant (see Fig. 5).

Fig. 6a plots $\frac{\beta}{\beta_0}$ vs. time (t) for live and dead cells with concentration of ρ = [10, 100, 1000] cells/µl. As cells metabolize in a nutritious environment, they uptake large molecules, such as glucose, and break them down to smaller species, such as lactic acid, which are much more conductive. As a result, R_{series} decreases with time. This process starts from the moment cells are in a new medium, i.e. live cells are metabolizing even in the lag-phase although their population is fixed (Rolfe et al., 2012). As cell size increases (starting in lag-phase), and eventually each cell divides into two identical daughter cells (in log-phase), R_{cell} increases. As such, in our system, the maximum sensitivity is achieved in the early stages of metabolism (within the first 60 min), as observed in Fig. 6a for live cells. On the other hand, there is almost no

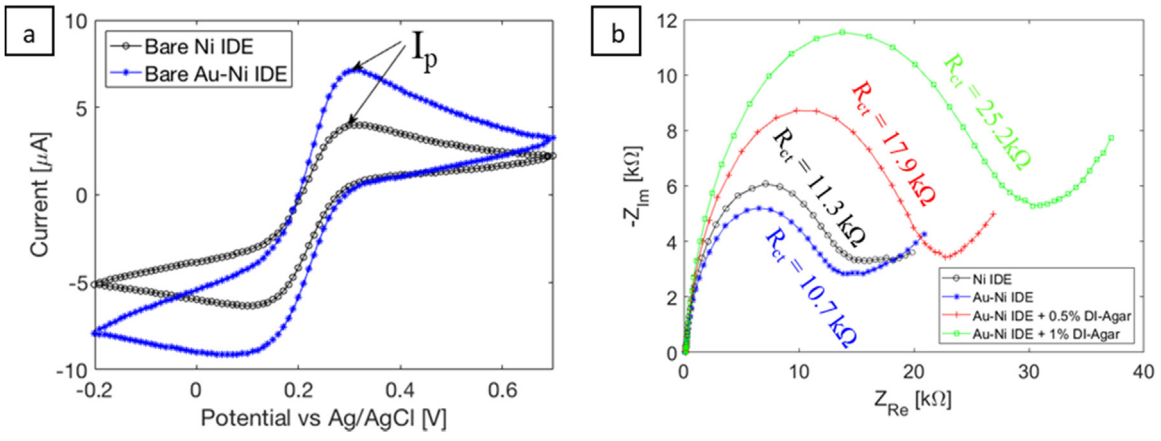

Fig. 3. (a) Cyclic voltammetry comparing bare Ni (black) and Au-Ni (blue) IDEs. The arrow indicates the peak current (I_p). $I_p^{Au-Ni}(blue) > I_p^{Ni}(black)$ indicating enhancement of the overall surface area after deposition of Au nanostructures. (b) Nyquist plots of the four device configurations are shown, in order of increasing the charge-transfer resistance, i.e. bare Au-Ni IDE (blue), bare Ni IDE (black), Au-Ni IDE with DI-agar 0.5% (red), and Au-Ni IDE with DI-agar 1% (green). Faradaic reaction is reduced by the increase of the agar concentration. In these experiments, the solution contains 5 mM of potassium ferricyanide in PBS×1, pH 7.2. (For interpretation of the references to color in this figure legend, the reader is referred to the web version of this article.).

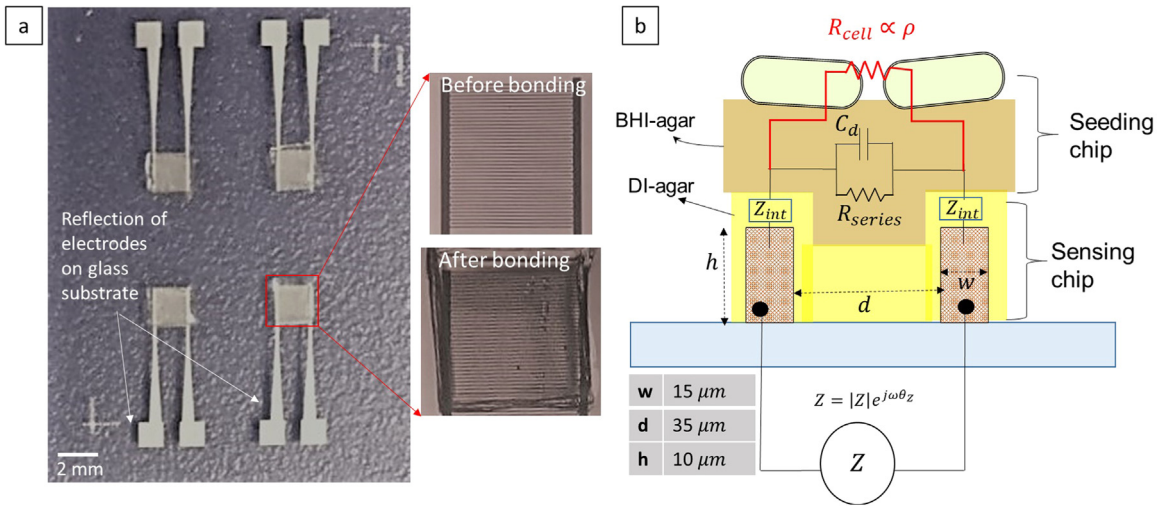

Fig. 4. (a) Optical image of an array of four biochips; inset shows 3D Au-Ni IDEs before and after bonding/integration with the seeding chip (BHI-agar pad). (b) Schematic of the biochip and the electrical circuit model (Z_{int}: interfacial impedance, R_{series}: medium resistance, C_d: dielectric capacitance, and R_{cell}: the resistance of bacterial cells). R_{series} decreases as cells metabolize and release metabolites. On the other hand, since live cells act as dielectric at working frequency of ~ 38 kHz, R_{cell} increases as they multiply (in log-phase). An AC voltage of 50 mV is applied and Z is measured at frequencies from 300 Hz to 2 MHz.

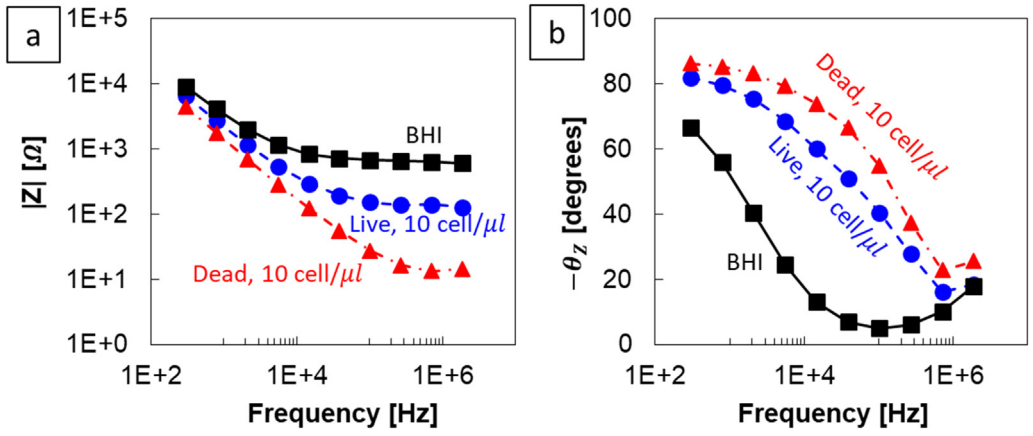

Fig. 5. (a) Impedance magnitude, $|Z|$, and (b) phase, θ_Z, for BHI (control sample) and live and heat-killed (dead) cells with concentration of 10 cells/μl after 45 min incubation. Compared to live cells with semipermeable membrane, dead cells have totally permeable membranes which results in leakage of cytoplasmic content to the medium. As such, impedance of dead cells is less than live cells.

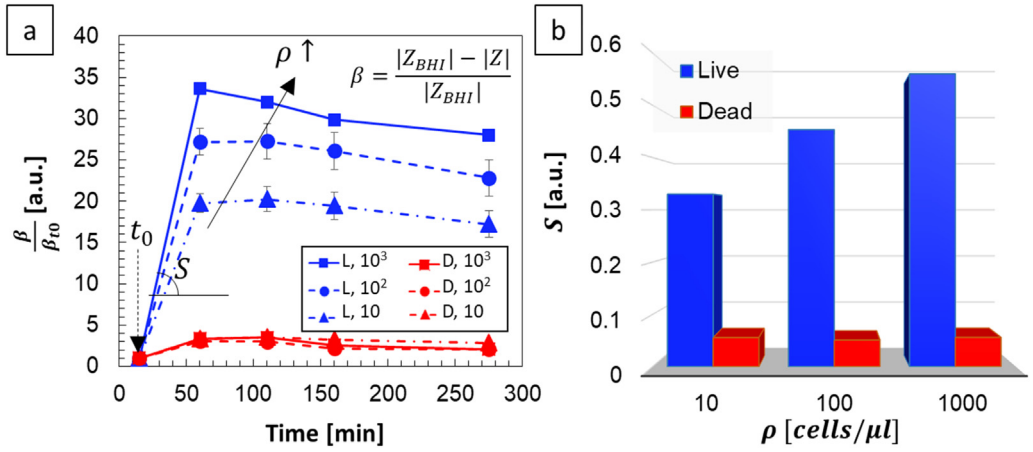

Fig. 6. (a) Normalized differential impedance (β/β_0 as defined in Eq. (2)) vs. time at working frequency of ~ 38 kHz, where medium resistance is dominant and the impedance change is maximum. L: Live cells, D: Dead cells. The sample concentrations are ρ = 10, 10^2, and 10^3 cells/μl. At least three replicates are measured for each sample condition. The error bars represent standard error from the averaged values. In some cases, the error bars are even smaller than the symbol size which demonstrate excellent robustness of the method. (b) The signal, S defined as the initial slope of β/β_0. The sensor response is linear over concentration range 10–1000 cells/μl.

signal change for dead cells due to the fact that after 15 min (where $\beta = \beta_0$), much of the heat-treated cells' cytoplasmic contents have already diffused out. As time increases, there is little change to the measured impedance for the heat-treated cells (i.e. $\frac{|Z(t)|}{|Z_{BHI}(t)|} \approx \frac{|Z(t_0)|}{|Z_{BHI}(t_0)|}$ at all times), and the signal remains nearly constant.

Plotted in Fig. 6b is the sensor sensitivity (defined as $S \equiv$ the initial slope of $\frac{\beta}{\beta_0}$ in Fig. 6a). As shown, the sensor offers an excellent selective response for differentiation of live, metabolizing *E. coli* cells, from non-metabolizing cells with a linear response in a concentration range of 10–1000 cells/μl. It is worth noting that conventional methods detect live bacterial cells as they enter the log- (or exponential) growth phase when cellular population increases rapidly (Bajwa et al., 2013). However, due to the significantly enhanced sensitivity of nanotextured 3D IDEs along with their close proximity to the metabolizing cells (due to stacking the BHI-agar right on the sensor surface), the developed biochip enables detection of cellular metabolism even in the lag-phase.

It should be noted that some pre-enrichment (e.g. initial culture) or array-formatted analysis (e.g. high throughput analysis of at least thousand pixels/sensors) may be required before being able to use the developed sensor in real scenarios, especially for food and water samples where the FDA-approved detection limit is only 1–10 cfu (colony forming unit)/ml (FDA, 2012). That said, the detection limit of the sensor developed in this work is readily within the acceptable range for application in early detection of urinary tract infection (UTI), where the clinically-relevant concentration for diagnostics is on the order of 10^4 cfu/ml (Hooton and Stamm, 1997). In addition, the detection limit reported in the present work is within the clinically-accepted concentration for determination of minimum inhibitory concentration (MIC) in antibacterial susceptibility testing assays, where the relevant concentration is on the order of 10^5 cfu/ml (Barth Reller et al., 2009).

4. Conclusion

In this work, we present a highly sensitive biochip for in situ detection of bacterial metabolism in *lag* phase. The sensor measures non-Faradaic impedance of 3D interdigitated microelectrodes integrated with gel-based bacterial culture in a highly compact platform. The designed 3D IDEs offer a significantly higher sensitivity compared to conventional thin film-based IDEs by having ~ 3 times larger sensing area, which is further augmented by incorporation of self-assembled gold nanostructures. In addition, the sensor sensitivity in measuring small changes of non-Faradaic impedance is enhanced by integrating a thin agar layer (which is dielectric) as a passivation layer. Through differential impedance calculations, *E. coli* concentrations of as low as 10^4 cells/ml, with a linear range of 10^4–10^6 cells/ml can be detected in approximately 60 min. This range is within the clinical requirement for UTI diagnostics, where a detection limit of $\sim 10^4$ cfu/ml is required. Moreover, the developed platform can potentially be integrated in rapid antibacterial susceptibility testing, as the clinically-relevant cell concentration should be $\sim 10^5$ cfu/ml. Further device/material optimization and integration of impedance sensing with array-formatted gel-based platforms could open up new possibilities for rapid, high-throughput pathogen detection, especially for food and water screening, where much lower detection limits are required.

Acknowledgment

The authors thank Dr. J. Robinson's group (Department of Materials Science and Engineering, PSU) for their help with the AFM characterization and Dr. J. Kovac's group (Department of Food Science, PSU) for their generous donation of *E. coli* K12 strains. This work is supported by the College of Engineering and the Materials Research Institute (MRI) at the Pennsylvania State University, and partially by a seed grant from MRI and Covestro Co.

Appendix A. Supporting information

Supplementary data associated with this article can be found in the online version at doi:10.1016/j.bios.2018.09.057.

References

Aperador Chaparro, W.A., Lopez, E.V., 2007. Electrodeposition of nickel plates on copper substrates using PC y PRC. Matér. (Rio De Jan.) 12 (4), 583–588.
Bajwa, A., Tan, S.T., Mehta, R., Bahreyni, B., 2013. Rapid detection of viable microorganisms based on a plate count technique using arrayed microelectrodes. Sensors 13, 8188–8198.
Balestra, G., Misaghi, I., 1997. Increasing the efficiency of the plate counting method for estimating bacterial diversity. J. Microbiol. Methods 30, 111–117.
Bard, A.J., Faulkner, L.R., 2001. Electrochemical Methods: Fundamentals and Applications, 2nd edition. John Wiley and Sons, Inc, New York.
Barth Reller, L., Weinstein, M., Jorgensen, J.H., Ferraro, M.J., 2009. Antimicrobial susceptibility testing: a review of general principles and contemporary practices. Clin. Infect. Dis. 49 (11), 1749–1755.
Bencko, V., 1983. Nickel: a review of its occupational and environmental toxicology. J. Hyg. Epidemiol. Microbiol. Immunol. 27 (2), 237–247.
Brownson, D.A.C., Banks, C.E., 2014. The Handbook of Graphene Electrochemistry.
Cempel, M., Nikel, G., 2006. Nickel: a review of its sources and environmental toxicology. Pol. J. Environ. Stud. 15, 375–382.
Creamer, K., et al., 2017. Benzoate- and salicylate-tolerant strains of *Escherichia coli* K-12 lose antibiotic resistance during laboratory evolution. Appl. Environ. Microbiol 83 (2).
Dak, P., Ebrahimi, A., Alam, M.A., 2014. Non-Faradaic impedance characterization of an evaporating droplet for microfluidic and biosensing applications. Lab Chip 14, 2469–2479.
Ebrahimi, A., Alam, M.A., 2015. Time-resolved PCA of "droplet impedance" identifies DNA hybridization at nM concentration. Sens. Actuators B Chem. 215, 215–224.
Ebrahimi, A., Alam, M.A., 2016. Evaporation-induced stimulation of bacterial osmoregulation for electrical assessment of cell viability. Proc. Natl. Acad. Sci. USA 113, 7059–7064.
Ebrahimi, A., Alam, M.A., 2017. Droplet-based non-Faradaic impedance sensors for assessment of susceptibility of Escherichia coli to ampicillin in 60 min. Biomed. Microdevices 19, 19–27.
Ebrahimi, A., Csonka, L.N., Alam, M.A., 2018. Analyzing thermal stability of cell membrane of salmonella using time-multiplexed impedance sensing. Biophys. J. 114, 609–618.
Ebrahimi, A., Dak, P., Salm, E., Dash, S., Garimella, S.V., Bashir, R., Alam, M.A., 2013. Nanotextured superhydrophobic electrodes enable detection of attomolar-scale DNA concentration within a droplet by non-Faradaic impedance spectroscopy. Lab a Chip 13, 4248–4256.
Environmental Protection Agency, 1997. Attachment I–Final Risk Assessment of Escherichia coli K-12 Derivatives.
Food and Drug Administration, 2012. Bad Bug Book, Foodborne Pathogenic Microorganisms and Natural Toxins, Second edition. .
Foxman, B., 2014. Urinary tract infection syndromes: occurrence, Recurrence, Bacteriology, risk factors, and disease burden. Infect. Dis. Clin. N. Am. 28 (1), 1–13.
Gómez, R., Bashir, R., Bhunia, A.K., 2002. Microscale electronic detection of bacterial metabolism. Sens. Actuators B Chem. 86, 198–208.
Gómez-sjöberg, R., Morisette, D.T., Bashir, R., Member, S., 2005. Impedance microbiology-on-a-chip: microfluidic bioprocessor for rapid detection of bacterial metabolism. J. Microelectromech. Syst. 14, 829–838.
Hooton, T.M., Stamm, W.E., 1997. Diagnosis and treatment of uncomplicated urinary tract infection. Infect. Dis. Clin. N. Am. 11 (3), 551–581.
Kurkina, T., Vlandas, A., Ahmad, A., Kern, K., Balasubramanian, K., 2011. Label-free detection of few copies of DNA with carbon nanotube impedance biosensors. Angew. Chem. - Int. 50, 3710–3714.
Levina, N., Tötemeyer, S., Stokes, N.R., Louis, P., Jones, M.A., Booth, I.R., 1999. Protection of Escherichia coli cells against extreme turgor by activation of MscS and MscL mechanosensitive channels: identification of genes required for MscS activity. EMBO J. 18, 1730–1737.
Mannoor, M.S., Zhang, S., Link, A.J., McAlpine, M.C., 2010. Electrical detection of pathogenic bacteria via immobilized antimicrobial peptides. Proc. Natl. Acad. Sci. USA 107, 19207–19212.
Min, J., Baeumner, A.J., 2004. Characterization and optimization of interdigitated ultramicroelectrode arrays as electrochemical biosensor transducers. Electroanalysis 16, 724–729.
Nazemi, E., Hassen, W.M., Frost, E.H., Dubowski, J.J., 2017. Monitoring growth and antibiotic susceptibility of Escherichia coli with photoluminescence of GaAs/AlGaAs quantum well microstructures. Biosens. Bioelectron. 93, 234–240.
Rolfe, M.D., Rice, C.J., Lucchini, S., Pin, C., Thompson, A., Cameron, A.D.S., Hinton, J.C.D., 2012. Lag phase is a distinct growth phase that prepares bacteria for exponential growth and involves transient metal accumulation. J. Bacteriol. 164, 686–701.
Shukla, R., Bansal, V., Chaudhary, M., Basu, A., Bhonde, R.R., Sastry, M., 2005. Biocompatibility of gold nanoparticles and their endocytotic fate inside the cellular compartment: a microscopic overview. Langmuir 21, 10644–10654.
Sidhu, R., Rong, Y., Vanegas, D.C., Claussen, J., McLamore, E.S., Gomes, C., 2016. Impedance biosensor for the rapid detection of *Listeria* spp. based on aptamer functionalized Pt-interdigitated microelectrodes array. Proceedings SPIE 9863, Smart

Biomedical and Physiological Sensor Technology XIII. 98630F.
Thomas, J.H., Kim, S.K., Hesketh, P.J., Halsall, H.B., Heineman, W.R., 2004. Microbead-based electrochemical immunoassay with interdigitated array electrodes. Anal. Biochem. 328, 113–122.
Varshney, M., Li, Y., 2009. Interdigitated array microelectrodes based impedance biosensors for detection of bacterial cells. Biosens. Bioelectron. 24, 2951–2960.
Xu, Y., Cai, H., He, P., Fang, Y., 2004. probing dna hybridization by impedance measurement based on CdS-oligonucleotide nanocojugates. Electroanalysis 16, 150–155.
Yang, L., Bashir, R., 2008. Electrical/electrochemical impedance for rapid detection of foodborne pathogenic bacteria. Biotechnol. Adv. 26, 135–150.
Zhang, S., Wang, N., Yu, H., Niu, Y., Sun, C., 2005. Covalent attachment of glucose oxidase to an Au electrode modified with gold nanoparticles for use as glucose biosensor. Bioelectrochemistry 67, 15–22.